

Insulator-Metal Transition and Topological Superconductivity in UTe_2 from a First-Principles Calculation

Jun Ishizuka, Shuntaro Sumita, Akito Daido, and Youichi Yanase

Department of Physics, Graduate School of Science, Kyoto University, Kyoto 606-8502, Japan

(Dated: November 4, 2019)

We theoretically study superconductivity in UTe_2 , which is a recently discovered strong candidate for an odd-parity spin-triplet superconductor. Theoretical studies for this compound faced difficulty because first-principles calculations predict an insulating electronic state, incompatible with superconducting instability. To overcome this problem, we take into account electron correlation effects by a GGA+ U method and show the insulator-metal transition by Coulomb interaction. Using Fermi surfaces obtained as a function of U , we clarify topological properties of possible superconducting states. Fermi surface formulas for the three-dimensional winding number and three two-dimensional \mathbb{Z}_2 numbers indicate topological superconductivity at an intermediate U for all the odd-parity pairing symmetry in the $Immm$ space group. Symmetry and topology of superconducting gap nodes are analyzed and the gap structure of UTe_2 is predicted. Topologically protected low-energy excitations are highlighted, and experiments by bulk and surface probes are proposed to link Fermi surfaces and pairing symmetry. Based on the results, we also discuss multiple superconducting phases under magnetic fields, which were implied by recent experiments.

A recent discovery of superconductivity in UTe_2 [1] is attracting much attention. Distinct differences of UTe_2 from other uranium-based ferromagnetic superconductors [2, 3] are a rather high superconducting transition temperature $T_c \sim 1.6$ K and a nonmagnetic behavior down to 25 mK [4]. Uniform magnetic susceptibility, magnetization, NMR Knight shift, and $1/T_1T$ support the proximity of metallic ferromagnetic quantum criticality [1, 5, 6]. An extremely large upper critical field and re-entrant superconductivity have been observed by high-field experiments [1, 7, 8]. These observations strongly suggest odd-parity superconductivity induced by ferromagnetic fluctuations. A large specific heat coefficient $\gamma = 117$ mJ K $^{-2}$ mol $^{-1}$ indicates itinerant heavy f electrons [5, 9, 10]. A large residual value of γ in the superconducting state [1, 5] suggests a time-reversal symmetry breaking nonunitary pairing, which is known to exist in ferromagnetic superconducting states. However, a direct transition from a normal to a nonunitary superconducting state is prohibited in the presence of spin-orbit coupling by symmetry because the orthorhombic D_{2h} point group of UTe_2 includes only one-dimensional (1D) representations. Experimental studies examining this issue are in progress.

Identifying the topological nature of quantum states has been one of the central issues in modern condensed matter physics. Because odd-parity superconductors are a strong candidate of topological superconductors accompanied by Majorana quasiparticles [11–13], many studies have been focused on the odd-parity superconductivity [14–16]. However, odd-parity superconducting materials are rare. Therefore, identifying topological properties of a fresh and good platform UTe_2 is awaited. A nonmagnetic behavior of UTe_2 enables time-reversal invariant (class DIII) topological superconductivity, and a relatively high transition temperature at ambient pressure allows many experimental tools, which were hard to use for ferromagnetic superconductors [2, 3]. Theoretically, it is important to specify Fermi surfaces (FSs) to identify topological superconductivity. Topological invariants

depend on FSs and some of them can be obtained by FS formulas [11–13].

Information on FSs can also be linked to gap structures of unconventional superconductors, and therefore, it enables us to study pairing symmetry by measurements of low energy excitations [17]. Recent progress in topological theory attached a renewed attention to the gap node. According to modern classification of gapless superconductors [18–21], all the superconducting gap nodes are topologically protected. Thus, the criterion of topological superconductivity and gap nodes based on FSs provides a prediction of bulk and surface measurements, revealing the pairing symmetry and Majorana surface states.

Theoretically, a band structure has been studied for UTe_2 from first-principles [5]. However, the previously obtained result shows an insulating state with a small gap of 13 meV, which contradicts metallic behaviors in electric resistivity [1, 5]. On the other hand, small FSs appear in another first-principles band calculation using the relativistic linearized augmented plane wave method [22]. This is also incompatible with transport measurements [23] indicating a large carrier density, as well as their angle-resolved photoemission spectroscopy (ARPES) detecting large intensities around the R point at the Fermi level [22]. These discrepancies between naive band structure calculations and experiments imply that the Coulomb interaction is crucially important for UTe_2 .

In this Letter, we provide the first report of a microscopic analysis linking the electronic state and superconductivity in UTe_2 . We show that the insulator-metal transition is induced by Coulomb interaction. For empirically reasonable values of U , a metallic state is realized, and FSs promise the topological superconductivity for all possible odd-parity pairings. The superconducting gap node ensured by crystal symmetry is predicted by the group theoretical classification combined with topological arguments. In addition, we discuss multiple superconducting phases under magnetic fields along the b axis. A phase transition inside the superconducting phase is

proposed.

GGA+ U calculation — The topology of the FS is crucially important for unconventional superconductors, in particular, for the gap structure and topological superconductivity. As we introduced previously, two band structures have been reported. One is insulating [5] and the other is metallic with small FSs [22]. They are clearly contradicting each other and incompatible with experiments. We therefore carry out the density functional theory (DFT) electronic structure calculations in the paramagnetic state using the WIEN2k package [24]. We use the relativistic full-potential linearized augmented plane wave + local orbitals method within the generalized gradient approximation (GGA). In addition to the DFT calculation providing a noninteracting band structure, we introduce the correlation effect of f electrons by the GGA+ U method [25]. Details of our band calculations are given in the Supplemental Material [26].

The numerical results are given in Figs. 1-2. The DFT band structure is insulating, and the band gap is 14 meV. Thus, the results are consistent with Ref. [5]. On the other hand, the GGA+ U calculation shows the closing of band gap (Fig. 1), and we observe metallic FSs for $U > 1.0$ eV. It turns out that the correlation effect of f electrons causes an insulator-metal transition. A moderate value of U in the GGA+ U calculation may be reliable at low temperatures, where the itinerant f electrons form a heavy fermion state consistent with specific heat measurements [1, 5]. A larger U may be appropriate above the Kondo temperature, where the f electrons are localized. Although we cannot determine the value of U in the framework of the GGA+ U method, we can deduce which FS is more appropriate using the comparison with future experiments such as ARPES or quantum oscillations. Furthermore, the GGA+ U calculation should be compared with other methods such as GGA+DMFT, which is left as a future work.

The obtained FSs are illustrated in Figs. 2(b)-2(d), each of which shows different topologies labeled by (i)-(iii) in Fig. 1(b). For $U = 1.0$ eV, a tiny electron sheet appears at the Brillouin zone (BZ) boundary around the X point and a tiny hole sheet around the R point. The FSs dramatically increase their volume by an increase of U , involving a topological Lifshitz transition from (i) to (ii). For $U = 1.1$ eV, there appears a ringlike sheet with a heavy effective mass dominated by $j_z = \pm 5/2$ and $\pm 1/2$ components [26]. We also see a cylindrical sheet dominated by $j_z = \pm 5/2$ and $\pm 3/2$ components. The ringlike sheet changes to a two-dimensional (2D) cylindrical sheet at $U = 2.0$ eV, which is shown in Fig. 2(d), with a topological transition at $U \simeq 1.6$ eV. These Fermi sheets consist of $j_z = \pm 5/2$ and $\pm 3/2$ components mixed with $d_{3z^2-r^2}$ and p_y orbitals having a light effective mass [26]. The electron sheet has a large carrier density $n \sim 0.2$ per spin which is compensated by the hole sheet. Thus, we see large FSs occupying 40% of the BZ, in accordance with transport measurements [23]. On the other hand, low carrier density shown in Fig. 2(b) or that obtained by a slight carrier doping to the DFT band structures is incompatible with experiments for UTe_2 . We also confirmed the insulator-metal

transition by the density of states [26]. Then, we notice that the incipient hybridization gap is shifted upwards in energy by 10 meV ($U = 1.0$ eV). The f -electron states with $j = 5/2$ multiplet are dominant around the Fermi level.

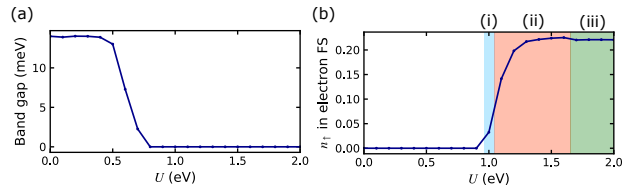


FIG. 1. Coulomb interaction dependence of (a) the band gap at the Fermi level and (b) the electron number n per spin in electron FS. Insulator-metal transition occurs at $U = 1.0$ eV. Metallic states with different topology of FSs are labeled by (i)-(iii).

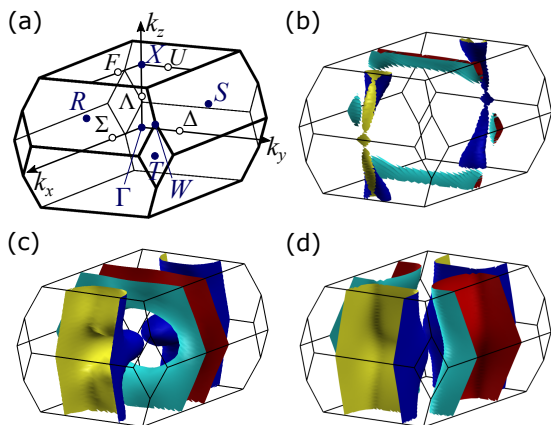


FIG. 2. (a) First BZ and symmetry points. (b)-(d) FSs of UTe_2 by GGA+ U for (b) $U = 1.0$ eV [region (i)], (c) $U = 1.1$ eV [region (ii)], and (d) $U = 2.0$ eV [region (iii)]. The electron sheet (cyan and red colors) and the hole sheet (blue and yellow colors) [26].

Topological superconductivity — Here, we discuss topological properties of UTe_2 , assuming odd-parity superconductivity. We also assume that time-reversal symmetry is preserved in the superconducting phase since this is natural from the group-theoretical perspective as discussed previously. Thus, we focus on the zero-magnetic-field phase and the putative nonunitary pairing state [1] is beyond our scope.

Topology of odd-parity superconductors is closely related to the topology of FSs. Actually, the parity of various topological invariants is determined by the occupation number at high-symmetry points in the BZ [11–13]. For example, we can identify the parity of the three-dimensional (3D) winding number ω by the following formula:

$$\omega = \frac{1}{2} \sum_{K_i} n(K_i) \pmod{2}. \quad (1)$$

Here, K_i runs over eight time-reversal invariant momenta (TRIM) in the 3D BZ, and the occupation number $n(K_i)$ is

TABLE I. Correspondence between high-symmetry points in the original BZ and folded BZ.

Original	Folded
Γ, X	$\Gamma_p : (0, 0, 0)$
R	$U_p : [(\pi/a), 0, (\pi/c)]$
S	$T_p : [0, (\pi/b), (\pi/c)]$
T	$S_p : [(\pi/a), (\pi/b), 0]$
W	$R_p : [(\pi/a), (\pi/b), (\pi/c)]$

an even integer due to Kramers degeneracy. Similar formulas are also known for 1D and 2D \mathbb{Z}_2 invariants [11–13].

In this Letter, we concentrate on topological invariants related to the (100), (010), and (001) surface states. It should be noted that the size of the primitive cell is doubled because the translation symmetry on these surfaces is compatible with the doubled unit cell. For this reason, we apply the formulas to the folded BZ, instead of the original one. To be specific, the former and the latter BZ correspond to the unit cell formed by $\{a\hat{x}, b\hat{y}, c\hat{z}\}$ and $\{(-a\hat{x} + b\hat{y} + c\hat{z})/2, (a\hat{x} - b\hat{y} + c\hat{z})/2, (a\hat{x} + b\hat{y} - c\hat{z})/2\}$, respectively. The correspondence between high-symmetry points in the two BZs is shown in Table I.

We obtained from the GGA+ U results the occupation number at TRIM and corresponding topological invariants (Table II). Here, ν_1 , ν_2 , and ν_3 are the \mathbb{Z}_2 invariants defined on the $k_x = 0$, $k_y = 0$, and $k_z = 0$ planes, respectively. \mathbb{Z}_2 invariants defined on the other time-reversal invariant planes are obtained from $(\omega, \nu_1, \nu_2, \nu_3)$, as is the case for topological insulators, and they are trivial in our results.

According to Table II, superconductivity in UTe_2 is topologically nontrivial for moderate values of U in the regions (i) and (ii) when the bulk state is gapped. Majorana states appear on the (100), (010), and (001) surfaces. This is one of the central results of this Letter.

Here we comment on the effect of excitation nodes on the topological superconductivity. Although the winding number ω is ill-defined in the gapless states, some of the 2D \mathbb{Z}_2 invariants ν_i may still be well defined and the corresponding surface Majorana states may appear. Well-defined topological invariants and surfaces hosting Majorana states are summarized in Table III for each pairing symmetry and FSs. For example, B_{1u} superconducting state has point nodes on the k_z axis, meaning ν_1 and ν_2 are ill-defined. However, ν_3 is well defined and (100) and (010) surface states are robust. Thus, topological superconductivity can be detected with scanning tunneling microscopy or ARPES for clean surfaces even in gapless superconducting states.

It should be noticed that our results do not exclude the possibility of topological superconductivity for FSs (iii): Indeed, 3D winding number $\omega \in \mathbb{Z}$ can be a finite even integer. By symmetry, this is allowed only for the A_u pairing state [27]. We do not discuss this case because ω depends on detailed properties of superconducting gap function. We also leave the possibility of topological crystalline superconductivity as a future issue.

TABLE II. Occupation number $n(K_i)$ at high symmetry points in the folded BZ and topological invariants (modulo two) corresponding to each topology of FSs. The values $n(K_i) - 180$ are shown below, with $X_p = (\pi/a, 0, 0)$, $Y_p = (0, \pi/b, 0)$, and $Z_p = (0, 0, \pi/c)$.

FSs	Γ_p	X_p	S_p	Y_p	Z_p	U_p	R_p	T_p	$(\omega, \nu_1, \nu_2, \nu_3)$
(i)	6	4	4	8	4	0	4	4	(1, 1, 1, 1)
(ii)	6	0	4	8	4	0	4	8	(1, 1, 1, 1)
(iii)	4	0	4	8	4	0	4	8	(0, 0, 0, 0)

Topological gap node — Now we discuss gap structures in the superconducting state of UTe_2 , using group theory and topology. First, we consider an ordinary classification theory of the superconducting *order parameter* by the crystal point group [17, 28–30]. At zero magnetic field, UTe_2 possesses D_{2h} point group symmetry, in which an odd-parity order parameter is classified as one of four irreducible representations (IRs): A_u , B_{1u} , B_{2u} , and B_{3u} . Typical basis functions are shown in Table IV(a). We also consider magnetic fields along the b axis in which UTe_2 shows extremely high critical fields and metamagnetic transition [1, 7–10]. Then, the symmetry is reduced to C_{2h}^y , which has two odd-parity IRs (A_u and B_u). In this case, the A_u and B_{2u} (B_{1u} and B_{3u}) states are not distinguished by symmetry since they are reduced to the A_u (B_u) state. The correspondence is summarized in Table IV(b).

Although we can speculate gap structures from the order parameter, it is desirable to use the classification of *gap structures* in terms of symmetry and topology [18–21, 31–37] because symmetry-protected gap nodes are precisely obtained. Detailed results of the topological classification are shown in the Supplemental Material [26]. Using the results, gap structures of UTe_2 are obtained for each pairing symmetry and FSs, as shown in Table III.

Considering the FS topology in Figs. 2(b)-2(d), we find that UTe_2 is a fully gapped superconductor at zero magnetic field when the order parameter belongs to A_u IR with $U > 1.0$ eV [regions (i)-(iii)], or B_{1u} IR with $U > 1.6$ eV [region (iii)]. Otherwise the superconducting state has some point nodes, whose positions depend on pairing symmetry and they can be distinguished by experiments. In Table V, we show expected anisotropy of thermal conductivity [38], which may determine the symmetry of superconductivity in UTe_2 .

When the magnetic field is applied along the b axis, superconducting states are classified into A_u or B_u IR. The A_u state of C_{2h}^y can be regarded as a $A_u + B_{2u}$ state, a mixed representation in D_{2h} , while $B_u \uparrow D_{2h} = B_{1u} + B_{3u}$. According to the gap classification in Table S2(b) of Supplemental Materials [26], the A_u state has symmetry-protected point nodes on the k_y axes while the B_u state has a line node on the $k_y = 0$ plane. These results are consistent with speculation from classification of order parameter. Since the spin-triplet order parameter with d -vector parallel to the magnetic field does not cause the gap of Bogoliubov quasiparticles, we have only to consider the others. For A_u IR, allowed bases are $k_x\hat{x}$, $k_z\hat{x}$, $k_x\hat{z}$, and $k_z\hat{z}$, which create point nodes. On the other hand,

TABLE III. Gap structures, nontrivial topological indices, and surfaces hosting stable Majorana states for odd-parity pairing states.

FSs(i,ii)				FSs(iii)			
IR	Gap structure	Topological index	Surfaces	IR	Gap structure	Topological index	Surfaces
A_u	Full gap	$(\omega, \nu_1, \nu_2, \nu_3)$	(100), (010), (001)	A_u	Full gap	$\omega \in 2\mathbb{Z}$	Unpredicted
B_{1u}	Point node (Λ)	ν_3	(100), (010)	B_{1u}	Full gap	Trivial	None
B_{2u}	Point node (Δ)	ν_2	(100), (001)	B_{2u}	Point node (Δ, U)	Trivial	None
B_{3u}	Point node (Σ, F)	ν_1	(010), (001)	B_{3u}	Point node (Σ, F)	Trivial	None

TABLE IV. Classification of odd-parity superconducting order parameters for point groups (a) D_{2h} and (b) C_{2h}^y .

(a) D_{2h} (zero magnetic field)									
IR	E	C_{2z}	C_{2y}	C_{2x}	I	σ_z	σ_y	σ_x	Basis functions
A_u	1	1	1	1	-1	-1	-1	-1	$k_x\hat{x}, k_y\hat{y}, k_z\hat{z}$
B_{1u}	1	1	-1	-1	-1	-1	1	1	$k_y\hat{x}, k_x\hat{y}$
B_{2u}	1	-1	1	-1	-1	1	-1	1	$k_x\hat{z}, k_z\hat{x}$
B_{3u}	1	-1	-1	1	-1	1	1	-1	$k_z\hat{y}, k_y\hat{z}$

(b) C_{2h}^y (magnetic field $\parallel b$)									
IR	(IR) $\uparrow D_{2h}$	E	C_{2y}	I	σ_y	Basis functions			
A_u	$A_u + B_{2u}$	1	1	-1	-1	$k_x\hat{x}, k_z\hat{x}, k_y\hat{y}, k_x\hat{z}, k_z\hat{z}$			
B_u	$B_{1u} + B_{3u}$	1	-1	-1	1	$k_y\hat{x}, k_x\hat{y}, k_z\hat{y}, k_y\hat{z}$			

TABLE V. Expected anisotropy in thermal conductivity at low temperatures for each FSs and pairing symmetry. Anisotropy of fully gapped states cannot be predicted.

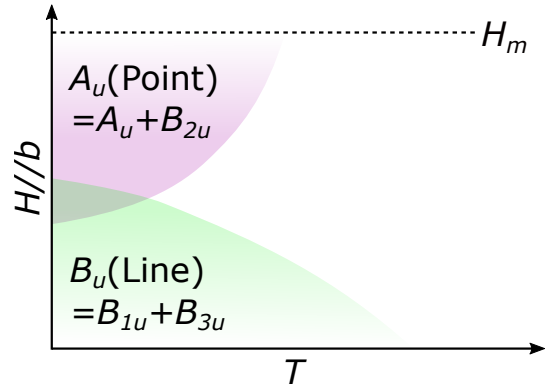
FSs	A_u	B_{1u}	B_{2u}	B_{3u}
(i)	Unpredicted	$\kappa_c > \kappa_{a,b}$	$\kappa_b > \kappa_{a,c}$	$\kappa_a > \kappa_{b,c}$
(ii)	Unpredicted	$\kappa_c > \kappa_{a,b}$	$\kappa_b > \kappa_{a,c}$	$\kappa_a > \kappa_{b,c}$
(iii)	Unpredicted	Unpredicted	$\kappa_b > \kappa_{a,c}$	$\kappa_a > \kappa_{b,c}$

the B_u order parameter of $k_y\hat{x}$ and $k_y\hat{z}$ results in line nodes on the $k_y = 0$ plane.

Multiple phases under magnetic fields — Experimental data for UTe_2 under magnetic fields along the b axis reveal highly unusual behaviors [1, 7, 8]. The transition temperature shows a nonmonotonic behavior as a function of the magnetic field. It indicates the presence of two superconducting phases: The low-field and high-field phases may be distinguished by symmetry. Considering the gap structure discussed above, we propose the phase diagram in Fig. 3. Because point-nodal superconducting states gain more condensation energy than line-nodal one, the A_u state may be stable at high magnetic fields, while the $B_u = B_{1u} + B_{3u}$ state may be favored by the spin-orbit coupling at low fields. In this case, the B_{1u} or B_{3u} state is realized at zero magnetic field. The order parameter of both states contains d -vector parallel to the b axis, and therefore, the Knight shift decreases below T_c . This is consistent with a recent NMR experiment [39].

Anisotropy of pairing interaction [40] is also important. Strongly anisotropic ferromagnetic fluctuation may favor the

d -vector perpendicular to the easy axis. Then, the easy axis along a [1] implies the B_{3u} state at $H = 0$ while the fluctuation along the b axis near the metamagnetic transition [9, 10] favors the B_{2u} state. This is consistent with our proposal. Microscopic calculations are desirable for more precise discussions and left for a future study.

FIG. 3. Schematic phase diagram in the magnetic field (H) and temperature (T) plane. H_m indicates the metamagnetic transition [9, 10].

Magnetism — Figures 2(c) and (d) show nesting property of the FSs, and therefore, we expect a magnetic fluctuation with a finite- q nesting vector coexisting with a widely believed ferromagnetic fluctuation. Thus, it is indicated that UTe_2 is in the vicinity of the multiple magnetic orderings, and the long-range magnetic order is suppressed by magnetic frustration. This may explain why UTe_2 does not undergo magnetic order in contrast to UCoGe and URhGe . A recent first-principles study proposes a similar scenario [41].

Summary and conclusion — In this Letter, we theoretically investigated the electronic state and superconductivity of UTe_2 . Using the GGA+ U calculation we clarified the insulator-metal transition due to Coulomb interaction. The metallic band structure for $U > 1.0$ eV is compatible with the metallic conductance and superconducting instability, indicating a crucial role of electron correlation. For moderate U , all the odd-parity superconducting states expected in UTe_2 were identified as time-reversal-invariant topological superconductivity. Superconducting gap structures under magnetic fields along the b axis as well as at zero magnetic field were predicted. By this work, bulk and surface excitations character-

izing the odd-parity superconductivity in UTe_2 are elucidated. Our results pave a way to experimentally determine symmetry of superconductivity and identify intrinsic topological superconductivity which has been rare in nature.

After we wrote the first manuscript, we become aware of Ref. [42], which reported DFT+ U calculations in both paramagnetic and ferromagnetic states. At their parameters $U = J = 0.51$ eV, an insulating band structure was obtained consistent with our calculations, and insulator-metal transition was not shown. We are also aware of an experimental paper [43] in which point nodes along the a axis are concluded. This implies the B_{3u} state at zero magnetic field consistent with our proposal in Fig. 3.

We appreciate helpful discussions with H. Ikeda, K. Izawa, K. Ishida, S. Fujimori, D. Aoki, and H. Harima. This work was supported by a Grant-in-Aid for Scientific Research on Innovative Areas “J-Physics” (Grant No. JP15H05884) and “Topological Materials Science” (Grants No. JP18H04225) from Japan Society for Promotion of Science (JSPS) and by JSPS KAKENHI (Grants No. JP15H05745, No. JP17H09908, No. JP17J10588, No. JP18H01178, and No. JP18H05227). Numerical calculations have been done at the supercomputer of the ISSP in Japan.

-
- [1] S. Ran, C. Eckberg, Q.-P. Ding, Y. Furukawa, T. Metz, S. R. Saha, I.-L. Liu, M. Zic, H. Kim, J. Paglione, and N. P. Butch, *Science* **365**, 684 (2019).
- [2] D. Aoki and J. Flouquet, *J. Phys. Soc. Jpn.* **83**, 061011 (2014).
- [3] D. Aoki, K. Ishida, and J. Flouquet, *J. Phys. Soc. Jpn.* **88**, 022001 (2019).
- [4] S. Sundar, S. Gheidi, K. Akintola, A. M. Côté, S. R. Dunsiger, S. Ran, N. P. Butch, S. R. Saha, J. Paglione, and J. E. Sonier, *Phys. Rev. B* **100**, 140502 (2019).
- [5] D. Aoki, A. Nakamura, F. Honda, D. Li, Y. Homma, Y. Shimizu, Y. J. Sato, G. Knebel, J.-P. Brison, A. Pourret, D. Braithwaite, G. Lapertot, Q. Niu, M. Vališka, H. Harima, and J. Flouquet, *J. Phys. Soc. Jpn.* **88**, 043702 (2019).
- [6] Y. Tokunaga, H. Sakai, S. Kambe, T. Hattori, N. Higa, G. Nakamine, S. Kitagawa, K. Ishida, A. Nakamura, Y. Shimizu, Y. Homma, D. Li, F. Honda, and D. Aoki, *J. Phys. Soc. Jpn.* **88**, 073701 (2019).
- [7] S. Ran, I.-L. Liu, Y. S. Eo, D. J. Campbell, P. M. Neves, W. T. Fuhrman, S. R. Saha, C. Eckberg, H. Kim, D. Graf, F. Balakirev, J. Singleton, J. Paglione, and N. P. Butch, *Nature Physics* (2019), 10.1038/s41567-019-0670-x.
- [8] G. Knebel, W. Knafo, A. Pourret, Q. Niu, M. Vališka, D. Braithwaite, G. Lapertot, M. Nardone, A. Zitouni, S. Mishra, I. Sheikin, G. Seyfarth, J.-P. Brison, D. Aoki, and J. Flouquet, *J. Phys. Soc. Jpn.* **88**, 063707 (2019).
- [9] W. Knafo, M. Vališka, D. Braithwaite, G. Lapertot, G. Knebel, A. Pourret, J.-P. Brison, J. Flouquet, and D. Aoki, *J. Phys. Soc. Jpn.* **88**, 063705 (2019).
- [10] A. Miyake, Y. Shimizu, Y. J. Sato, D. Li, A. Nakamura, Y. Homma, F. Honda, J. Flouquet, M. Tokunaga, and D. Aoki, *J. Phys. Soc. Jpn.* **88**, 063706 (2019).
- [11] M. Sato, *Phys. Rev. B* **79**, 214526 (2009).
- [12] M. Sato, *Phys. Rev. B* **81**, 220504(R) (2010).
- [13] L. Fu and E. Berg, *Phys. Rev. Lett.* **105**, 097001 (2010).
- [14] X.-L. Qi and S.-C. Zhang, *Rev. Mod. Phys.* **83**, 1057 (2011).
- [15] M. Sato and S. Fujimoto, *J. Phys. Soc. Jpn.* **85**, 072001 (2016).
- [16] M. Sato and Y. Ando, *Rep. Prog. Phys.* **80**, 076501 (2017).
- [17] M. Sigrist and K. Ueda, *Rev. Mod. Phys.* **63**, 239 (1991).
- [18] S. Kobayashi, K. Shiozaki, Y. Tanaka, and M. Sato, *Phys. Rev. B* **90**, 024516 (2014).
- [19] S. Kobayashi, Y. Yanase, and M. Sato, *Phys. Rev. B* **94**, 134512 (2016).
- [20] S. Kobayashi, S. Sumita, Y. Yanase, and M. Sato, *Phys. Rev. B* **97**, 180504(R) (2018).
- [21] S. Sumita, T. Nomoto, K. Shiozaki, and Y. Yanase, *Phys. Rev. B* **99**, 134513 (2019).
- [22] S.-i. Fujimori, I. Kawasaki, Y. Takeda, H. Yamagami, A. Nakamura, Y. Homma, and D. Aoki, *J. Phys. Soc. Jpn.* **88**, 103701 (2019).
- [23] Q. Niu, G. Knebel, D. Braithwaite, D. Aoki, G. Lapertot, G. Seyfarth, J.-P. Brison, J. Flouquet, and A. Pourret, “Fermi-Surface Instabilities in the Heavy-Fermion Superconductor UTe_2 ,” [arXiv:1907.11118](https://arxiv.org/abs/1907.11118).
- [24] P. Blaha, K. Schwarz, G. K. H. Madsen, D. Kvasnicka, J. Luitz, R. Laskowski, F. Tran, and L. D. Marks, *WIEN2k, An Augmented Plane Wave + Local Orbitals Program for Calculating Crystal Properties* (Karlheinz Schwarz, Techn. Universität Wien, Austria, 2018).
- [25] V. I. Anisimov, J. Zaanen, and O. K. Andersen, *Phys. Rev. B* **44**, 943 (1991).
- [26] See Supplemental Material for details, which includes Refs. [44–53].
- [27] T. Yoshida, A. Daido, N. Kawakami, and Y. Yanase, *Phys. Rev. B* **99**, 235105 (2019).
- [28] G. E. Volovik and L. P. Gor’kov, *Pis’ma Zh. Eksp. Teor. Fiz.* **39**, 550 (1984).
- [29] G. E. Volovik and L. P. Gor’kov, *Zh. Eksp. Teor. Fiz.* **88**, 1412 (1985).
- [30] P. W. Anderson, *Phys. Rev. B* **30**, 4000 (1984).
- [31] V. G. Yarzhevsky and E. N. Murav’ev, *J. Phys.: Condens. Matter* **4**, 3525 (1992).
- [32] M. R. Norman, *Phys. Rev. B* **52**, 15093 (1995).
- [33] T. Micklitz and M. R. Norman, *Phys. Rev. B* **80**, 100506(R) (2009).
- [34] T. Nomoto and H. Ikeda, *J. Phys. Soc. Jpn.* **86**, 023703 (2017).
- [35] T. Micklitz and M. R. Norman, *Phys. Rev. Lett.* **118**, 207001 (2017).
- [36] S. Sumita, T. Nomoto, and Y. Yanase, *Phys. Rev. Lett.* **119**, 027001 (2017).
- [37] S. Sumita and Y. Yanase, *Phys. Rev. B* **97**, 134512 (2018).
- [38] R. Joynt and L. Taillefer, *Rev. Mod. Phys.* **74**, 235 (2002).
- [39] G. Nakamine, S. Kitagawa, K. Ishida, Y. Tokunaga, H. Sakai, S. Kambe, A. Nakamura, Y. Shimizu, Y. Homma, D. Li, F. Honda, and D. Aoki, *J. Phys. Soc. Jpn.* **88**, 113703 (2019).
- [40] Y. Yanase, T. Jujo, T. Nomura, H. Ikeda, T. Hotta, and K. Yamada, *Phys. Rep.* **387**, 1 (2003).
- [41] Y. Xu, Y. Sheng, and Y. feng Yang, “Quasi-two-dimensional Fermi surfaces and unitary spin-triplet pairing in the heavy fermion superconductor UTe_2 ,” [arXiv:1908.07396](https://arxiv.org/abs/1908.07396).
- [42] A. B. Shick and W. E. Pickett, *Phys. Rev. B* **100**, 134502 (2019).
- [43] T. Metz, S. Bae, S. Ran, I.-L. Liu, Y. S. Eo, W. T. Fuhrman, D. F. Agterberg, S. Anlage, N. Butch, and J. P. Paglione, “Point Node Gap Structure of Spin-Triplet Superconductor UTe_2 ,” [arXiv:1908.01069](https://arxiv.org/abs/1908.01069).
- [44] A. J. K. Haneveld and F. Jellinek, *J. Less Common Metals* **21**, 45 (1970).
- [45] M. T. Czyżyk and G. A. Sawatzky, *Phys. Rev. B* **49**, 14211

- (1994).
- [46] V. I. Anisimov, I. V. Solovyev, M. A. Korotin, M. T. Czyżyk, and G. A. Sawatzky, *Phys. Rev. B* **48**, 16929 (1993).
 - [47] A. I. Liechtenstein, V. I. Anisimov, and J. Zaanen, *Phys. Rev. B* **52**, R5467 (1995).
 - [48] E. P. Wigner, *Group Theory and Its Application to the Quantum Mechanics of Atomic Spectra* (Academic Press, New York, 1959).
 - [49] C. Herring, *Phys. Rev.* **52**, 361 (1937).
 - [50] T. Inui, Y. Tanabe, and Y. Onodera, *Group Theory and Its Applications in Physics*, Springer Series in Solid-State Sciences, Vol. 78 (Springer-Verlag Berlin Heidelberg, Berlin, Heidelberg, 1990).
 - [51] C. J. Bradley and A. P. Cracknell, *The Mathematical Theory of Symmetry in Solids* (Oxford University Press, Oxford, 1972).
 - [52] K. Shiozaki, M. Sato, and K. Gomi, “Atiyah-hirzebruch spectral sequence in band topology: General formalism and topological invariants for 230 space groups,” [arXiv:1802.06694](https://arxiv.org/abs/1802.06694).
 - [53] A. Altland and M. R. Zirnbauer, *Phys. Rev. B* **55**, 1142 (1997).

Supplemental Materials:
Insulator-Metal Transition and Topological Superconductivity in UTe₂
from a First-Principles Calculation

S1. DETAILS OF BAND CALCULATION

We perform the DFT band structure calculation in the paramagnetic state of UTe₂ using the WIEN2k code [S1]. The crystallographical parameters are shown in Table S1 [S2]. UTe₂ crystallizes in an orthorhombic body-centered structure (space group No. 71, *Immm*) and the local site symmetry of uranium atoms is C_{2v} , lacking the inversion symmetry. The maximum reciprocal lattice vector K_{\max} was given by $R_{\text{MT}}K_{\max} = 11.0$. The muffin-tin radii R_{MT} of 2.50 a.u. was chosen for U and Te atoms, and $12 \times 12 \times 12$ k -points sampling was used for the self-consistent calculation. For the GGA+ U calculation, we set Hund's coupling $J = 0$ eV. We use the around mean-field formula [S3] for the double-counting correlation, and we crosschecked results with the self-interaction correction formula [S4, S5].

Figure S1 shows the band structure by DFT and GGA+ U along high symmetry lines. Uranium $5f$ orbitals split into the $j = 5/2$ and $j = 7/2$ manifolds due to the spin-orbit coupling. We observe near the Fermi level doubly degenerated bands of the $j = 5/2$ multiplet, two of which are valence bands, and other four bands are conduction bands. The $j = 7/2$ states are located at around 1.0 eV. The electron occupancy of $5f$ orbitals is around $n_f \sim 2.5$, which is larger than the nominal occupancy of U²⁺ ion $n_f^0 = 2$. Note that the dispersive bands at around -0.5 eV are composed of $5f$ orbitals mixed with U- $d_{3z^2-r^2}$ orbital and Te(2)- p_y orbital. The DFT band structure is consistent with the previous result [S6]. Moreover, in Fig. S1, j_z orbital characters are highlighted. The $j_z = \pm 1/2, \pm 3/2$, and $\pm 5/2$ states are quite entangled. The flat bands near the band gap are dominated by $j_z = \pm 1/2$ and $\pm 5/2$ states in the DFT calculation. The band structures by GGA+ U are shown for $U = 1.0, 1.1$, and 2.0 eV. Compared to the DFT results, two $j = 5/2$ bands are shifted downward in energy about $U/2$, leaving the band structure near the Fermi level dominated by the $5f$ $j_z = \pm 5/2$ and $\pm 3/2$ states. We can see an electron pocket at the S and X points and a hole pocket at the R point. Figure S2 shows partial density of states for U- $5f$ orbitals $j = 5/2, j_z = \pm 1/2, \pm 3/2$, and $\pm 5/2$ near the Fermi level. We can confirm the insulator-metal transition. The $j_z = \pm 5/2$ states are dominated at the Fermi level for $U = 1.0$ and 1.1 eV.

TABLE S1. Atomic coordinates of UTe₂. Lattice constants are $a = 4.1617$, $b = 6.1276$, and $c = 13.9650$ Å.

Atom	x	y	z
U ($4i$)	0	0	0.13480
Te1 ($4j$)	0.5	0	0.29770
Te2 ($4h$)	0	0.2510	0.5

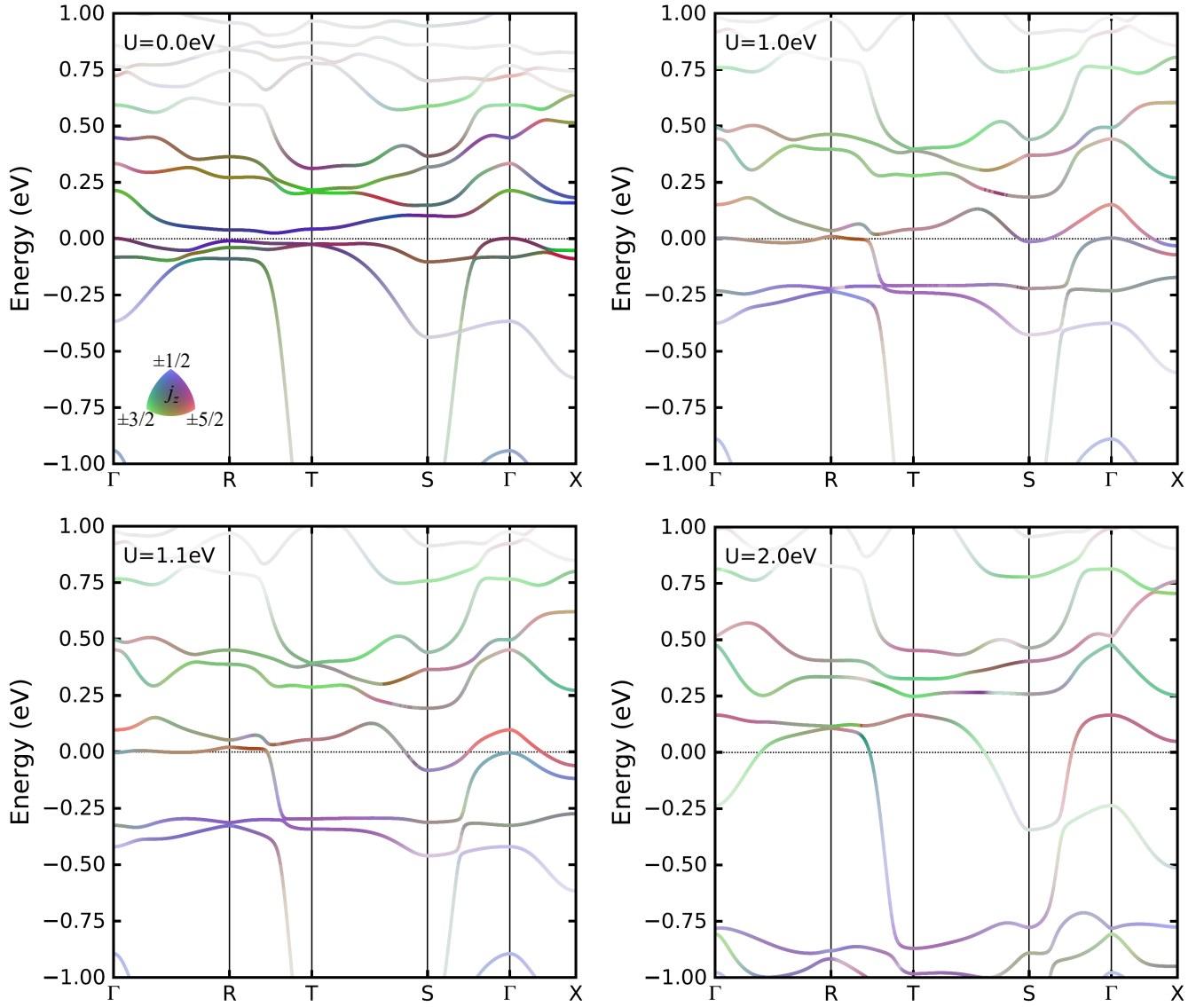


FIG. S1. The calculated band structure by the DFT and GGA+ U along the high symmetry line. Compared to the DFT results, two $j = 5/2$ bands are pushed downward in energy about $U/2$, leaving the band structure near the Fermi level dominated by the $5f$ $j_z = \pm 5/2$ and $\pm 3/2$ states. The blue, green, red, and grey colors represent the weight of orbitals for $j_z = \pm 1/2$, $\pm 3/2$, $\pm 5/2$, and other components, respectively.

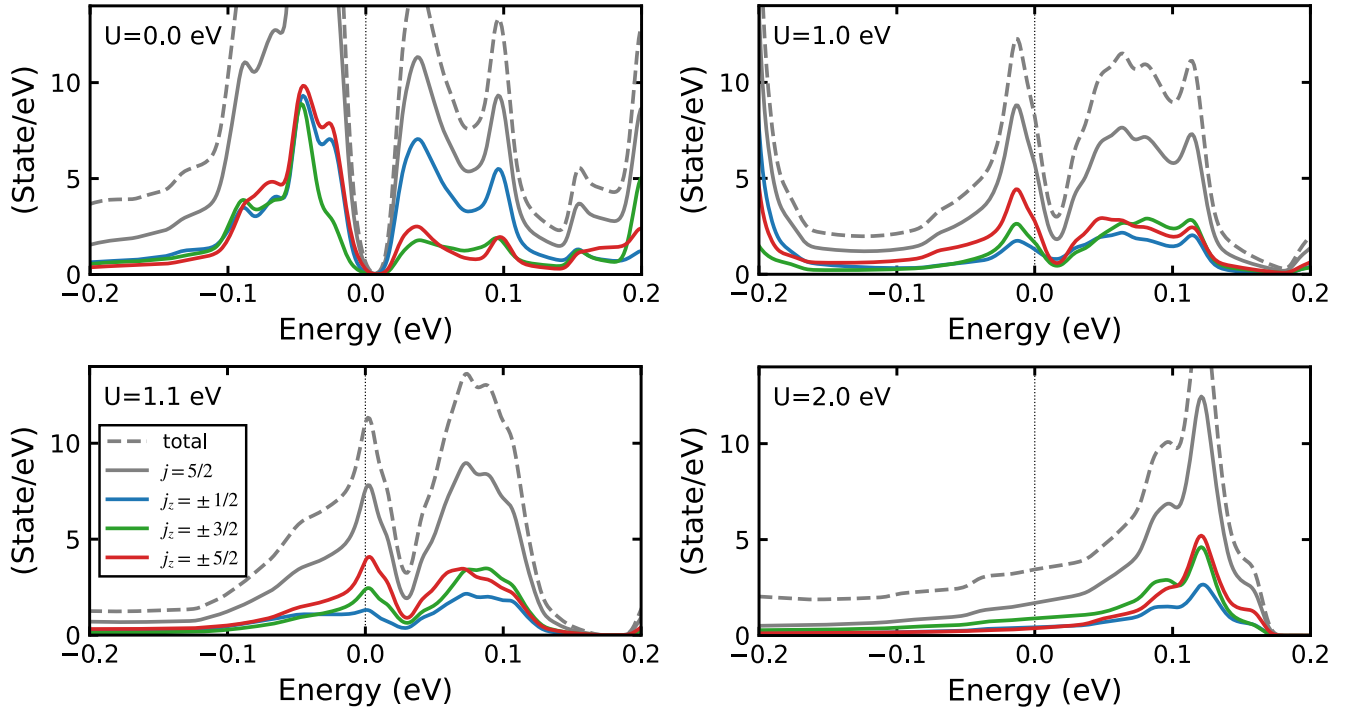


FIG. S2. Partial density of states for U-5*f* orbitals $j = 5/2$, $j_z = \pm 1/2, \pm 3/2$, and $\pm 5/2$ near the Fermi level. Dashed line represents the total density of states.

TABLE S2. Classification of superconducting gap structures on mirror planes and rotational axes under (a) zero magnetic field and (b) magnetic fields along the b axis. In the tables, we show the EAZ class for each pairing symmetry. Letters in parenthesis represent the absence (0) or presence (\mathbb{Z} or \mathbb{Z}_2) of a topological invariant, and gap structures: (G) full gap, (P) point nodes, or (L) line nodes.

(a) Zero magnetic field							(b) Magnetic field $\parallel b$		
D_{2h}	$k_z = 0, 2\pi/c$	$k_y = 0$	$k_x = 0$	k_z axis (Δ)	k_y axes (Δ, U)	k_x axes (Σ, F)	C_{2h}^y	$k_y = 0$	k_y axes (Δ, U)
A_u	C (0, G)	C (0, G)	C (0, G)	CI (0, G)	CI (0, G)	CI (0, G)	A_u	C (0, G)	AI (\mathbb{Z} , P)
B_{1u}	C (0, G)	AIII (0, G)	AIII (0, G)	BDI (\mathbb{Z}_2 , P)	CI (0, G)	CI (0, G)	B_u	A (\mathbb{Z} , L)	CI (0, G)
B_{2u}	AIII (0, G)	C (0, G)	AIII (0, G)	CI (0, G)	BDI (\mathbb{Z}_2 , P)	CI (0, G)			
B_{3u}	AIII (0, G)	AIII (0, G)	C (0, G)	CI (0, G)	CI (0, G)	BDI (\mathbb{Z}_2 , P)			

S2. TOPOLOGICAL CLASSIFICATION OF SUPERCONDUCTING GAP STRUCTURES

Table IV in the main text gives a classification of superconducting *order parameter*, which enables us to speculate gap structures of UTe_2 . However, it is desirable to use the classification of *gap structures* in terms of symmetry and topology [S7–S17] because symmetry-protected gap nodes are precisely obtained. This scheme focuses on high-symmetry points in the Brillouin zone in Fig. 2(a) of the main text: mirror planes ($k_z = 0, 2\pi/c, k_y = 0$, and $k_x = 0$) and rotational axes labeled by $\Delta, \Delta, U, \Sigma$, and F . Crystal symmetry allowed on each high-symmetry \mathbf{k} point is represented by a unitary little cogroup $\bar{\mathcal{G}}^{\mathbf{k}}$, whose irreducible representation is denoted by α .

At zero magnetic field, we define time-reversal symmetry (TRS), particle-hole symmetry (PHS), and chiral symmetry (CS) operators preserving any \mathbf{k} points by $\mathfrak{T} \equiv \mathcal{TI}$, $\mathfrak{C} \equiv \mathcal{CI}$, and $\Gamma \equiv \mathcal{TC}$, respectively. Thus the intrinsic symmetry is represented by the following group:

$$\bar{\mathfrak{G}}^{\mathbf{k}} = \bar{\mathcal{G}}^{\mathbf{k}} + \mathfrak{T}\bar{\mathcal{G}}^{\mathbf{k}} + \mathfrak{C}\bar{\mathcal{G}}^{\mathbf{k}} + \Gamma\bar{\mathcal{G}}^{\mathbf{k}}. \quad (\text{S1})$$

Then, using the factor system $\{z_{g,h}^{\mathbf{k}}\} \in Z^2(\bar{\mathfrak{G}}^{\mathbf{k}}, \text{U}(1)_\phi)$, we execute the *Wigner criteria* [S18–S22] for \mathfrak{T} and \mathfrak{C} , and the *orthogonality test* [S20, S22] for Γ :

$$W_\alpha^\mathfrak{T} \equiv \frac{1}{|\bar{\mathcal{G}}^{\mathbf{k}}|} \sum_{g \in \bar{\mathcal{G}}^{\mathbf{k}}} z_{\mathfrak{T}g, \mathfrak{T}g}^{\mathbf{k}} \chi[\bar{\gamma}_\alpha^{\mathbf{k}}((\mathfrak{T}g)^2)] = \begin{cases} 1, \\ -1, \\ 0, \end{cases} \quad (\text{S2})$$

$$W_\alpha^\mathfrak{C} \equiv \frac{1}{|\bar{\mathcal{G}}^{\mathbf{k}}|} \sum_{g \in \bar{\mathcal{G}}^{\mathbf{k}}} z_{\mathfrak{C}g, \mathfrak{C}g}^{\mathbf{k}} \chi[\bar{\gamma}_\alpha^{\mathbf{k}}((\mathfrak{C}g)^2)] = \begin{cases} 1, \\ -1, \\ 0, \end{cases} \quad (\text{S3})$$

$$W_\alpha^\Gamma \equiv \frac{1}{|\bar{\mathcal{G}}^{\mathbf{k}}|} \sum_{g \in \bar{\mathcal{G}}^{\mathbf{k}}} \frac{z_{g, \Gamma^{-1}g}^{\mathbf{k}*}}{z_{\Gamma^{-1}g, \Gamma}^{\mathbf{k}*}} \chi[\bar{\gamma}_\alpha^{\mathbf{k}}(\Gamma^{-1}g\Gamma)^*] \chi[\bar{\gamma}_\alpha^{\mathbf{k}}(g)] = \begin{cases} 1, \\ 0. \end{cases} \quad (\text{S4})$$

From Eqs. (S2)-(S4), we obtain the set of $(W_\alpha^\mathfrak{T}, W_\alpha^\mathfrak{C}, W_\alpha^\Gamma)$, which indicates the *effective* Altland-Zirnbauer (EAZ) symmetry class of the Bogoliubov-de Gennes Hamiltonian on the high-symmetry point [S22, S23]. The EAZ class gives us classification of gap structures, assuming that the high-symmetry planes or lines intersect normal-state Fermi surfaces (for details, see Ref. [S17]). After some algebra, we obtain the gap classification shown in Table S2(a).

Under magnetic field along the b axis, on the other hand, the intrinsic symmetry is changed. On the mirror plane ($k_y = 0$), TRS \mathfrak{T} and CS Γ are ill-defined, while PHS \mathfrak{C} is introduced by \mathcal{CI} . On the rotational axes (Δ, U), we define TRS, PHS, and CS by $\mathfrak{T} \equiv \mathcal{TC}_{2z}$, $\mathfrak{C} \equiv \mathcal{CI}$, and $\Gamma \equiv \mathcal{TC}_{2z}\mathcal{CI}$, respectively. Eqs. (S2)-(S4) are also applied into the cases, which result in Table S2(b). Note that $W_\alpha^\mathfrak{T} = W_\alpha^\Gamma = 0$ on the mirror plane since the little cogroup $\bar{\mathfrak{G}}^{\mathbf{k}}$ has *no* TRS and CS.

[S1] P. Blaha, K. Schwarz, G. Madsen, D. Kvasnicka, and J. Luitz, WIEN2k, An Augmented Plane Wave + Local Orbitals Program for Calculating Crystal Properties (Tech. Univ. Wien, Vienna, 2001).

[S2] A. J. K. Haneveld and F. Jellinek, *J. Less Common Metals* **21**, 45 (1970).

[S3] M. T. Czyżyk and G. A. Sawatzky, *Phys. Rev. B* **49**, 14211 (1994).

[S4] V. I. Anisimov, I. V. Solovveyev, M. A. Korotin, M. T. Czyżyk, and G. A. Sawatzky, *Phys. Rev. B* **48**, 16929 (1993).

- [S5] A. I. Liechtenstein, V. I. Anisimov, and J. Zaanen, *Phys. Rev. B* **52**, R5467 (1995).
- [S6] D. Aoki, A. Nakamura, F. Honda, D. Li, Y. Homma, Y. Shimizu, Y. J. Sato, G. Knebel, J.-P. Brison, A. Pourret, D. Braithwaite, G. Lapertot, Q. Niu, M. Vališka, H. Harima, and J. Flouquet, *J. Phys. Soc. Jpn.* **88**, 043702 (2019).
- [S7] V. G. Yarzhemsky and E. N. Murav'ev, *J. Phys.: Condens. Matter* **4**, 3525 (1992).
- [S8] M. R. Norman, *Phys. Rev. B* **52**, 15093 (1995).
- [S9] T. Micklitz and M. R. Norman, *Phys. Rev. B* **80**, 100506(R) (2009).
- [S10] T. Nomoto and H. Ikeda, *J. Phys. Soc. Jpn.* **86**, 023703 (2017).
- [S11] T. Micklitz and M. R. Norman, *Phys. Rev. Lett.* **118**, 207001 (2017).
- [S12] S. Sumita, T. Nomoto, and Y. Yanase, *Phys. Rev. Lett.* **119**, 027001 (2017).
- [S13] S. Sumita and Y. Yanase, *Phys. Rev. B* **97**, 134512 (2018).
- [S14] S. Kobayashi, K. Shiozaki, Y. Tanaka, and M. Sato, *Phys. Rev. B* **90**, 024516 (2014).
- [S15] S. Kobayashi, Y. Yanase, and M. Sato, *Phys. Rev. B* **94**, 134512 (2016).
- [S16] S. Kobayashi, S. Sumita, Y. Yanase, and M. Sato, *Phys. Rev. B* **97**, 180504(R) (2018).
- [S17] S. Sumita, T. Nomoto, K. Shiozaki, and Y. Yanase, *Phys. Rev. B* **99**, 134513 (2019).
- [S18] E. P. Wigner, *Group Theory and its Application to the Quantum Mechanics of Atomic Spectra* (Academic Press, New York, 1959).
- [S19] C. Herring, *Phys. Rev.* **52**, 361 (1937).
- [S20] T. Inui, Y. Tanabe, and Y. Onodera, *Group theory and its applications in physics*, Springer Series in Solid-State Sciences, Vol. 78 (Springer-Verlag Berlin Heidelberg, Berlin, Heidelberg, 1990).
- [S21] C. J. Bradley and A. P. Cracknell, *The Mathematical Theory of Symmetry in Solids* (Oxford University Press, Oxford, 1972).
- [S22] K. Shiozaki, M. Sato, and K. Gomi, "Atiyah-hirzebruch spectral sequence in band topology: General formalism and topological invariants for 230 space groups," [arXiv:1802.06694](https://arxiv.org/abs/1802.06694).
- [S23] A. Altland and M. R. Zirnbauer, *Phys. Rev. B* **55**, 1142 (1997).